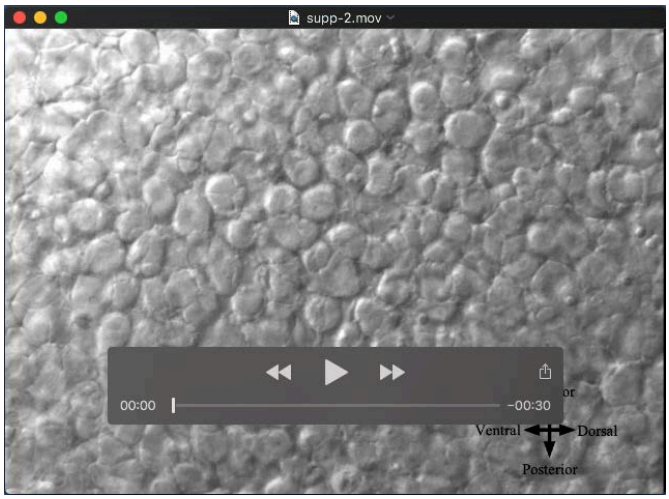

Movie 1. The onset of dorsal convergence. DIC time-lapse imaging of wild-type lateral hypoblast/mesendodermal cells located 90° from the notochord and near the embryo equator as shown in Fig. 2A (15 min time-lapse/30 s imaging intervals). Anterior is to the top and dorsal to the right. At the beginning of imaging, the embryo is at approximately the 75% epiboly stage. The cells initially migrate anteriorly and then make an abrupt right turn toward the dorsal body axis.

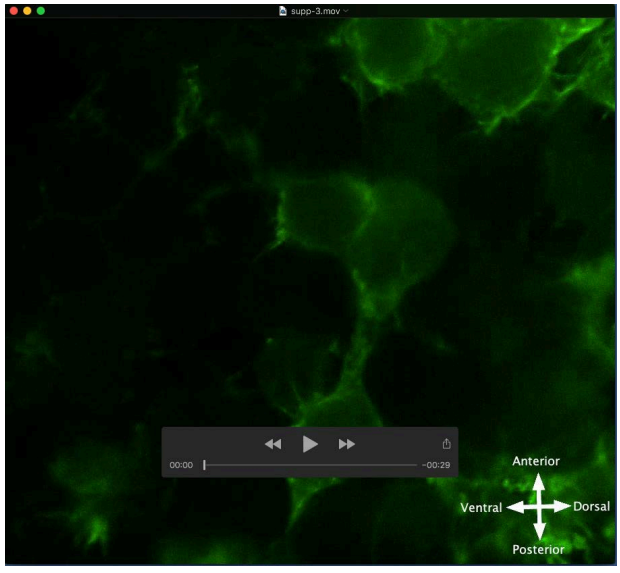

Movie 2. Wild-type embryo + Lifeact-GFP mRNA at 80% epiboly. Confocal time-lapse imaging of hypoblast/mesendodermal cells located 90° from the notochord and near the embryo equator as shown in Fig. 2A (15 min time-lapse/1 min imaging intervals). Anterior is to the top and dorsal to the right.

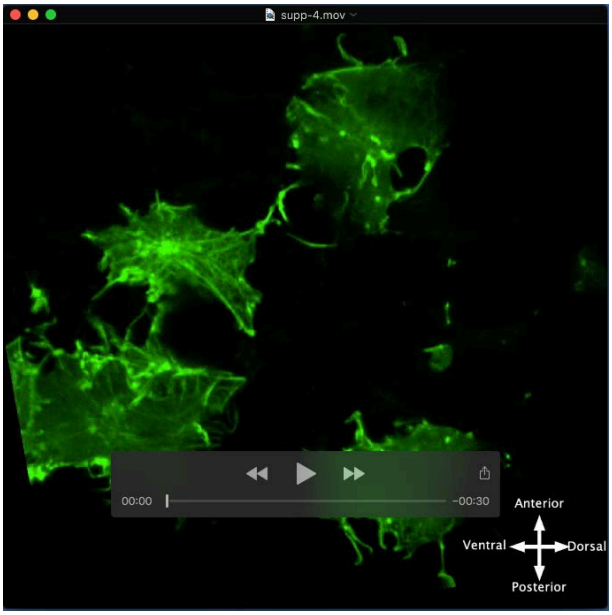

Movie 3. Wild-type embryo + Lifeact-GFP mRNA at ypc/tb. Confocal time-lapse imaging of mesodermal cells located 90° from the notochord and near the embryo equator as shown in Fig. 2A (15 min time-lapse/1 min imaging intervals). Anterior is to the top and dorsal to the right.

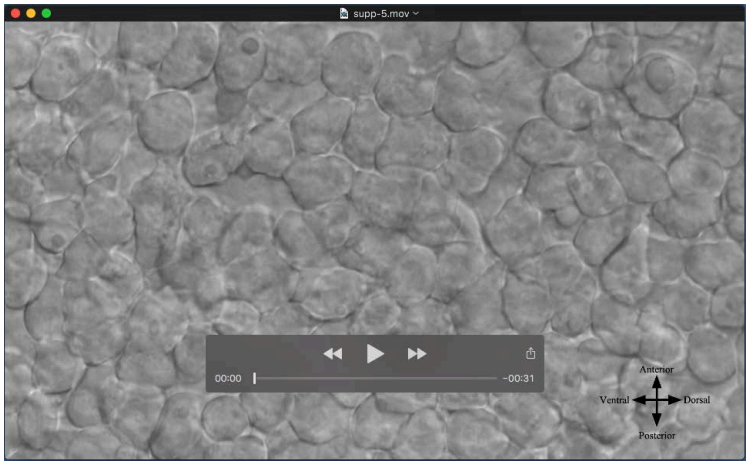

Movie 4. Wild-type embryo at 80% epiboly. DIC time-lapse imaging of hypoblast/ mesendodermal cells located 90° from the notochord and near the embryo equator as shown in Fig. 2A (15 min time-lapse/30 s imaging intervals). Anterior is to the top and dorsal to the right. Select bleb protrusions are highlighted with arrowheads.

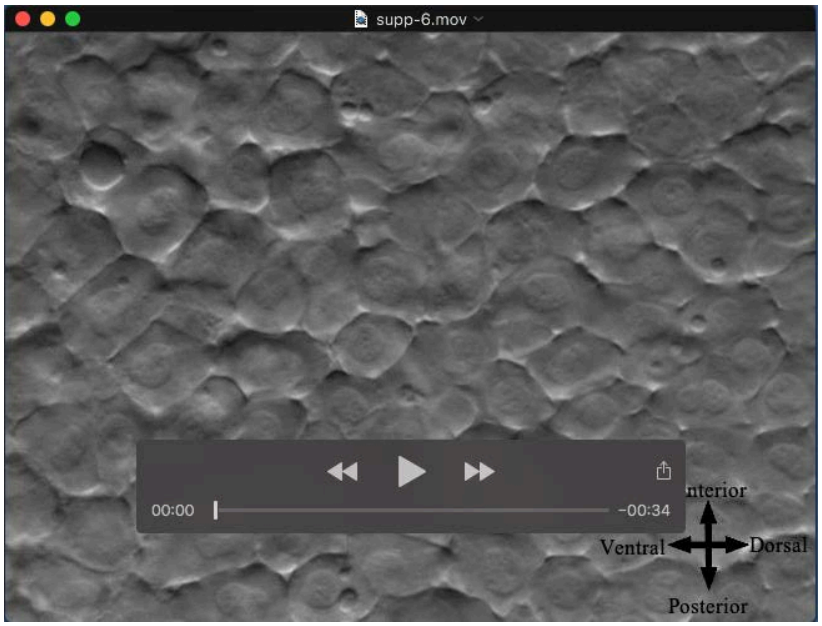

Movie 5. Wild-type embryo at ypc/tb. DIC time-lapse imaging of mesodermal cells located 40-60° from the notochord and near the embryo equator as shown in Fig. 2A (15 min time-lapse/30 s imaging intervals). Anterior is to the top and dorsal to the right. Select bleb protrusions are highlighted with arrowheads.

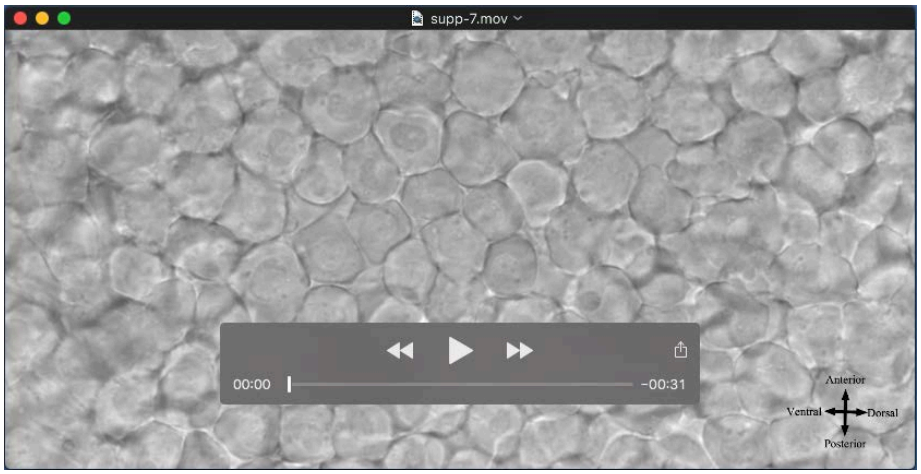

Movie 6. Wild-type embryo + ca-*ezrb* mRNA at 80% epiboly. DIC time-lapse imaging of hypoblast/mesendodermal cells located 90° from the notochord and near the embryo equator as shown in Fig. 2A (15 min time-lapse/30 s imaging intervals). Anterior is to the top and dorsal to the right. Select bleb protrusions are highlighted with arrowheads.

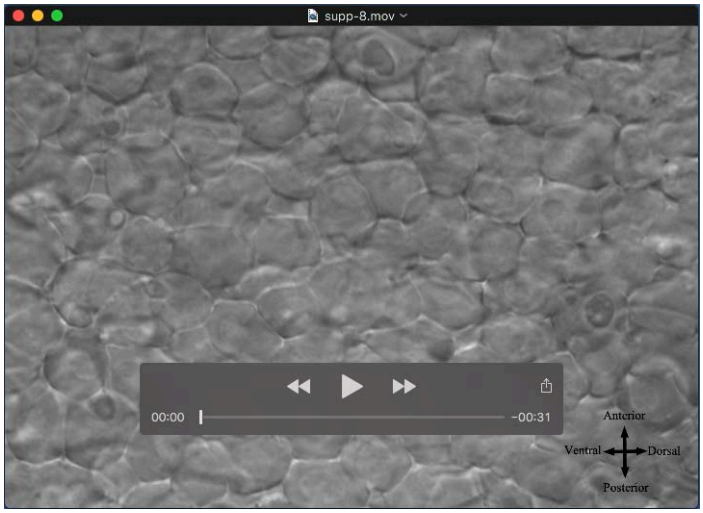

Movie 7. Wild-type embryo + *ezrb* MO at ypc/tb. DIC time-lapse imaging of mesodermal cells located 40-60° from the notochord and near the embryo equator as shown in Fig. 2A (15 min time-lapse/30 s imaging intervals). Anterior is to the top and dorsal to the right. Select bleb protrusions are highlighted with arrowheads.

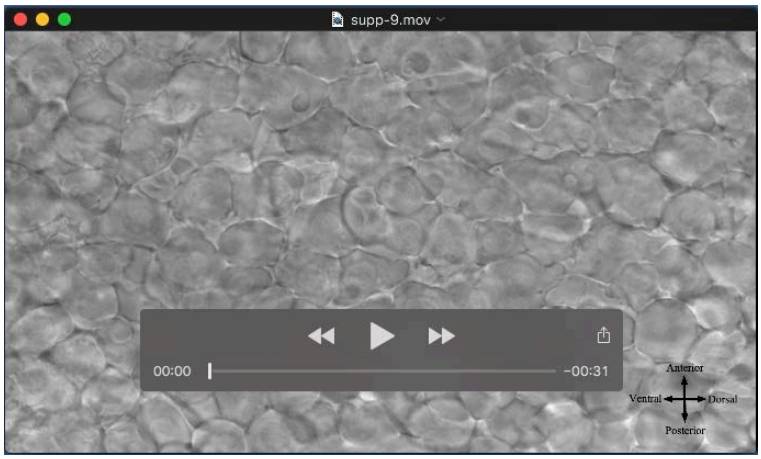

Movie 8. Wild-type embryo + *fn1a/1b* MO at ypc/tb. DIC time-lapse imaging of mesodermal cells located 40-60° from the notochord and near the embryo equator as shown in Fig. 2A (15 min time-lapse/30 s imaging intervals). Anterior is to the top and dorsal to the right. Select bleb protrusions are highlighted with arrowheads.

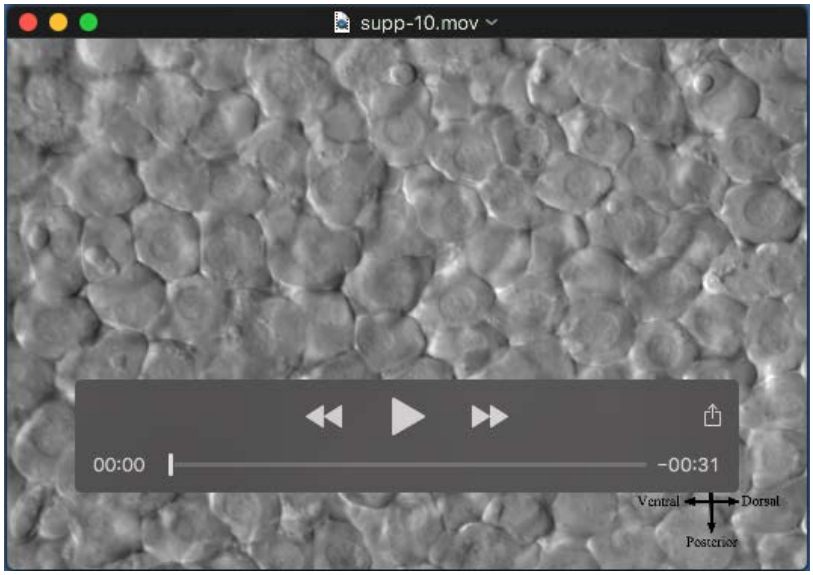

Movie 9. Wild-type embryo + *cdh2* MO at ypc/tb. DIC time-lapse imaging of mesodermal cells located 40-60° from the notochord and near the embryo equator as shown in Fig. 2A (15 min time-lapse/30 s imaging intervals). Anterior is to the top and dorsal to the right. Select bleb protrusions are highlighted with arrowheads.

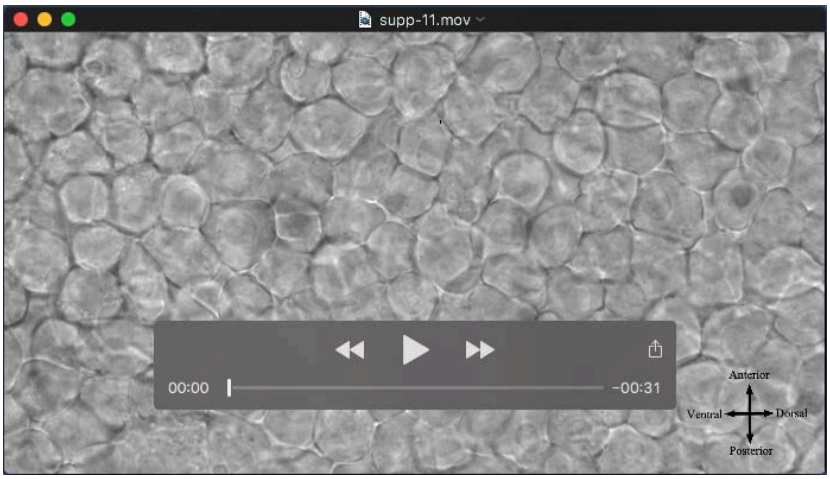

Movie 10. Wild-type embryo + *fn1a/1b* mRNA at 80% epiboly. DIC time-lapse imaging of hypoblast/mesendodermal cells located 90° from the notochord and near the embryo equator as shown in Fig. 2A (15 min time-lapse/30 s imaging intervals). Anterior is to the top and dorsal to the right. Select bleb protrusions are highlighted with arrowheads.

Movie 11. ***vangl2*$^{vu67/vu67}$ mutant embryo at ypc/tb.** DIC time-lapse imaging of mesodermal cells located 40-60° from the notochord and near the embryo equator as shown in Fig. 2A (15 min time-lapse/30 s imaging intervals). Anterior is to the top and dorsal to the right. Select bleb protrusions are highlighted with arrowheads.

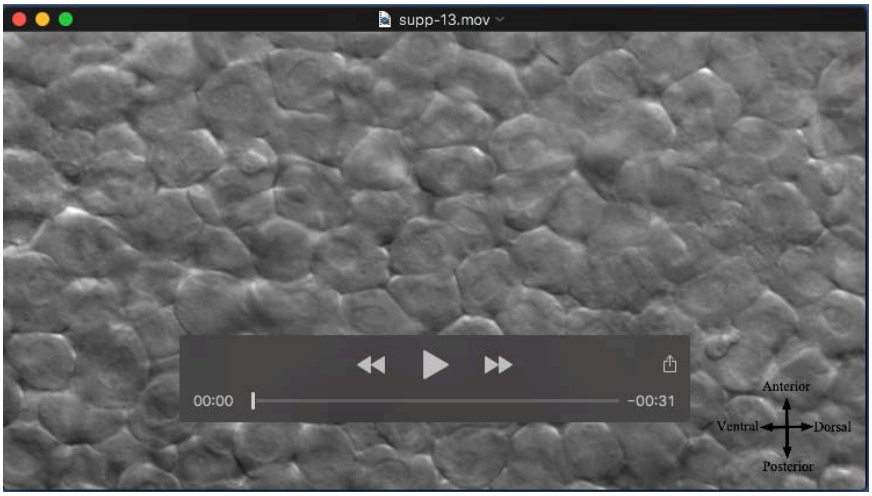

Movie 12. ***vangl2*$^{vu67/vu67}$ mutant embryo + ca-*ezrb* mRNA at ypc/tb.** DIC time-lapse imaging of mesodermal cells located 40-60° from the notochord and near the embryo equator as shown in Fig. 2A (15 min time-lapse/30 s imaging intervals). Anterior is to the top and dorsal to the right. Select bleb protrusions are highlighted with arrowheads.

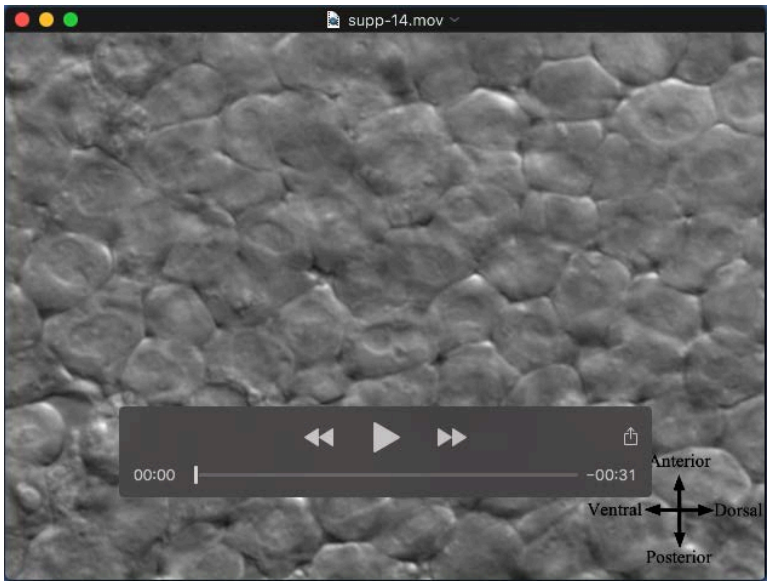

Movie 13. ***vangl2*$^{vu67/vu67}$ mutant embryo + *fn1a/1b* mRNA at ypc/tb.** DIC time-lapse imaging of mesodermal cells located 40-60° from the notochord and near the embryo equator as shown in Fig. 2A (15 min time-lapse/30 s imaging intervals). Anterior is to the top and dorsal to the right. Select bleb protrusions are highlighted with arrowheads.

Fig. S1. Schematic diagrams of methods used to quantify protrusion polarity and PCP. (A) Filopodia and large lamellipodia-like protrusion polarity were determined in relation to dorsal-ventral body axis. Protrusions were arbitrarily considered aligned if they were oriented +/- 45° relative to the dorsal-ventral axis. (B) Since bleb protrusions were examined at 80% epiboly, the stage when wild-type mesendodermal cells meander toward the dorsal body axis, polarity was determined in relation to the individual cell migration path. Paths were determined by following the frames from time-lapse movies. Lines were drawn through the cell center along the path of movement and through the center of the bleb protrusion and the angles were obtained. Bleb protrusions were arbitrarily considered aligned if they were oriented +/- 45° relative to the path of migration. (C) The length-width ratio of gastrula cells was determined by dividing cell length by cell width as measured at the greatest distances. A value of ~1.6 is found in wild-type lateral mesodermal cells at late gastrulation; a value of ~1.3 is typical for *vangl2* mutants. (D) Mediolateral alignment is calculated by measuring the angle between lines drawn along the dorsal-ventral body axis and the long axis of the cell. Cells were considered aligned if their long axis is oriented +/- 20° relative to the dorsal-ventral axis.

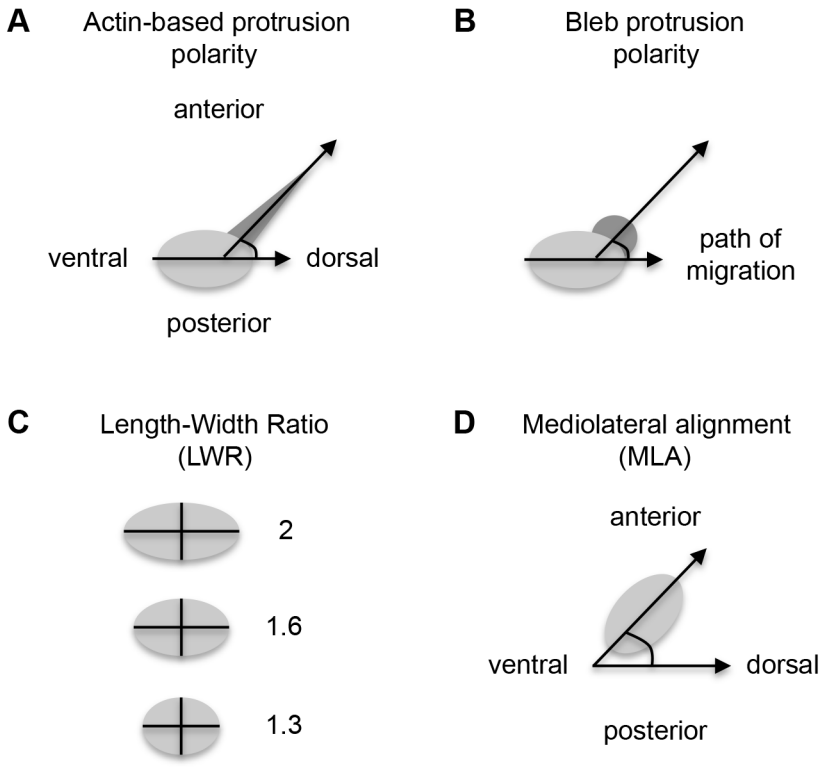

Fig. S2. *ezrb* morpholino injected embryos have mediolaterally broadened mesoderm. Live embryo and whole-mount in situ hybridization (WISH) images of ypc/tb stage embryos. Dorsal views with anterior to the top. Black lines denote notochord (arrow) widths near the embryonic equator of live embryos. White lines highlight the width of paraxial/lateral mesoderm as shown by *protocadherin 8* (*pcdh8*) staining. n, notochord. The *ezrb* morphant paraxial/lateral mesoderm is approximately 10% wider than controls.

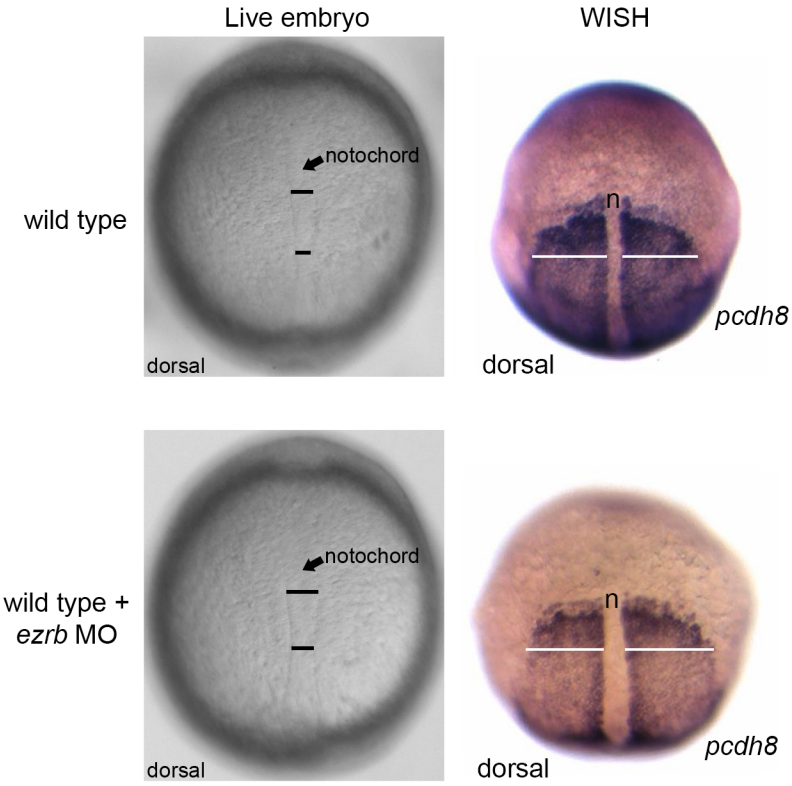

Fig. S3. DIC time-lapse image series showing bleb formation at the ypc/tb stage. Depicted are representative images from our time-lapse analyses of wild type control and morphant embryos. Images shown are separated by 30 s time intervals and white arrows denote forming and retracting bleb protrusions. Images are oriented with anterior to the top and dorsal to the right. Scale bars, 5 μm.

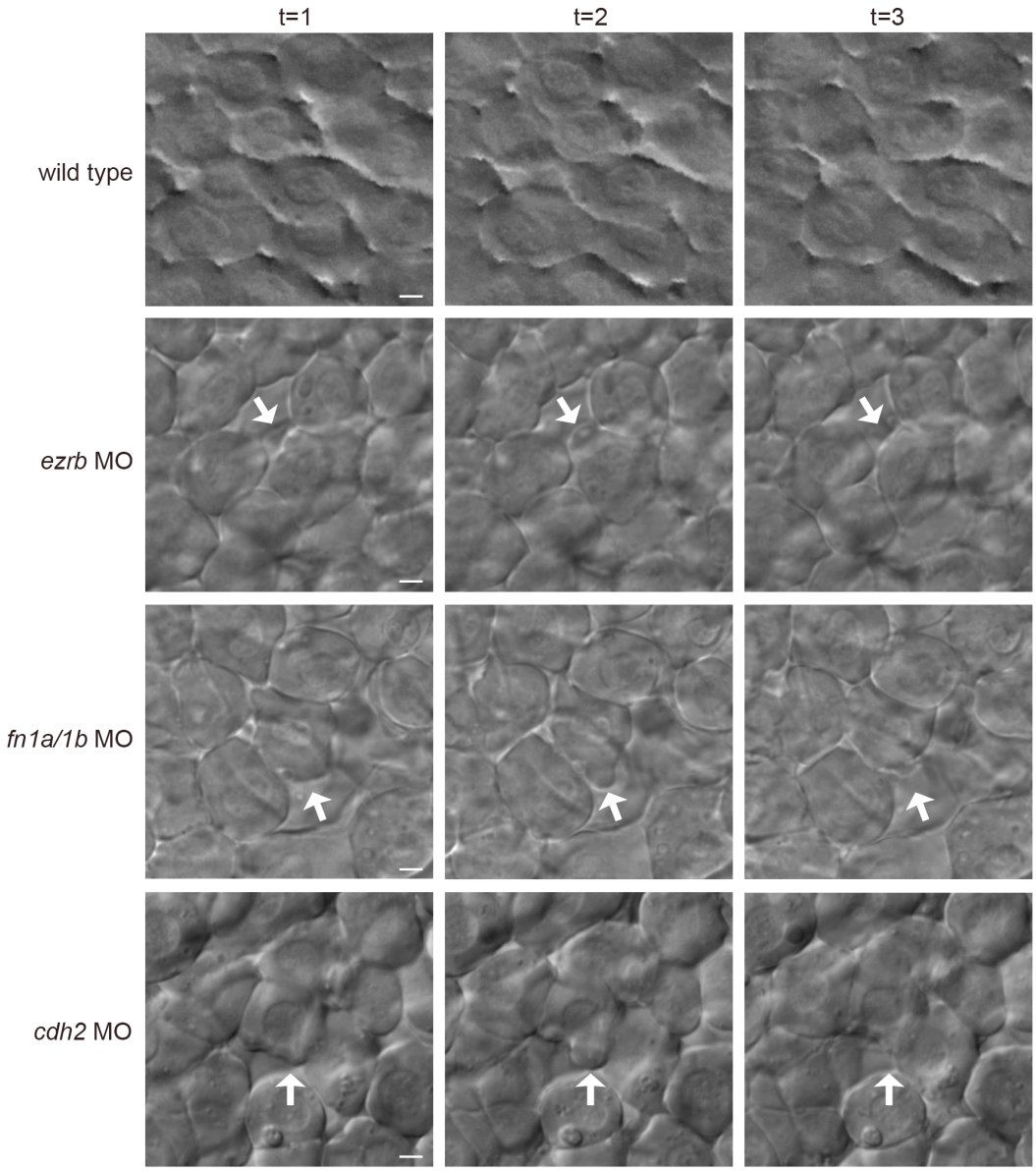

Fig. S4. DIC time-lapse image series showing bleb formation at the 80% epiboly stage. Depicted are representative images from our time-lapse analyses of wild type control and mRNA injected embryos. Images shown are separated by 30 s time intervals and white arrows denote forming and retracting bleb protrusions. Images are oriented with anterior to the top and dorsal to the right. Scale bars, 5 μm.

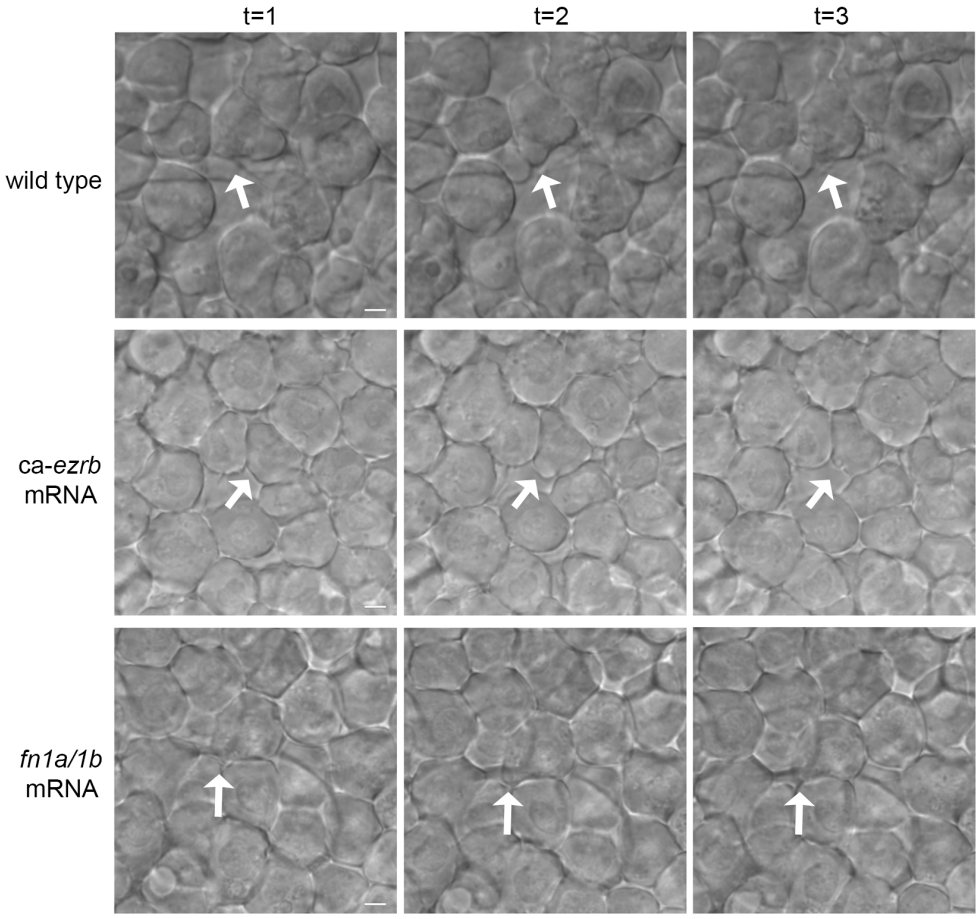

Fig. S5. DIC time-lapse image series showing bleb formation at the ypc/tb stage. Depicted are representative images from our time-lapse analyses of *vangl2* mutant control and mRNA injected embryos. Images shown are separated by 30 s time intervals and white arrows/arrowheads denote forming and retracting bleb protrusions. Images are oriented with anterior to the top and dorsal to the right. Scale bars, 5 μm.

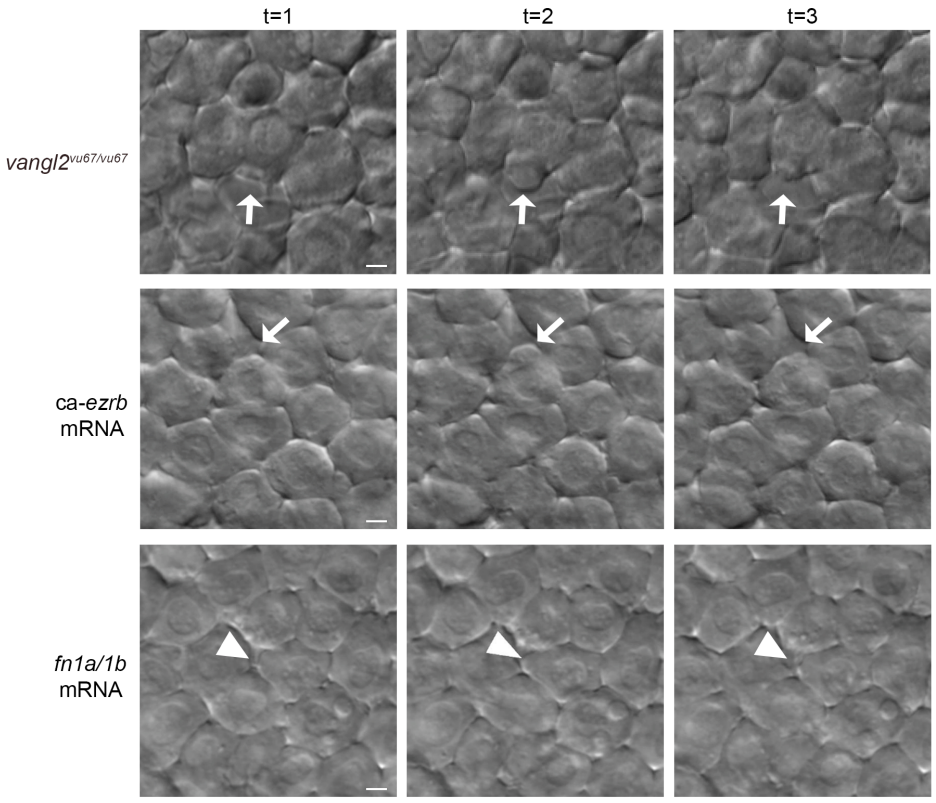

Fig. S6. Bleb protrusions per cell. Quantitation of the number of blebs formed per cell for wild type, mRNA/MO injected, and mutant embryos. Box plots show the interquartile dataset, the median, and the data range. *P<0.05, **P<0.01; unpaired Student's t-test with Welch's correction.

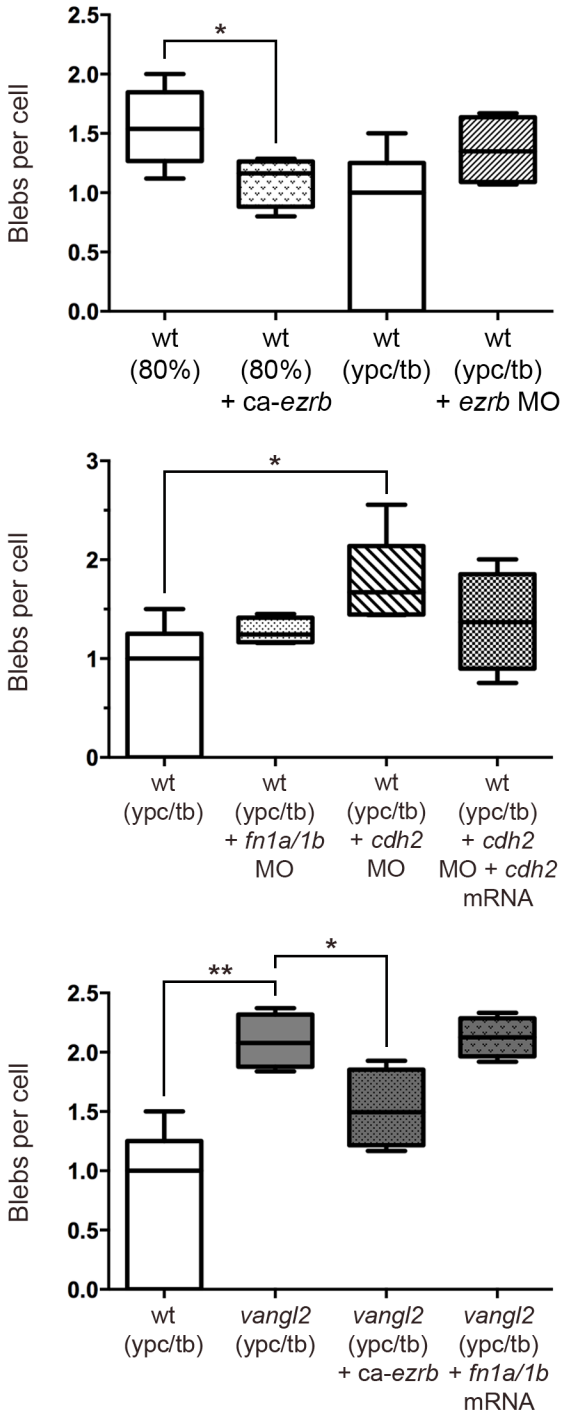

Fig. S7. Rose diagrams depicting MLA of gastrula cells. Bidirectional Rose diagrams correspond to the MLA angular data shown in Figs 4D, 5E, and 7B. The size of the gray shading indicates cell number at specific angles. Mesendodermal (80% epiboly) and mesodermal (yolk plug-closure/tailbud) cell data are shown.

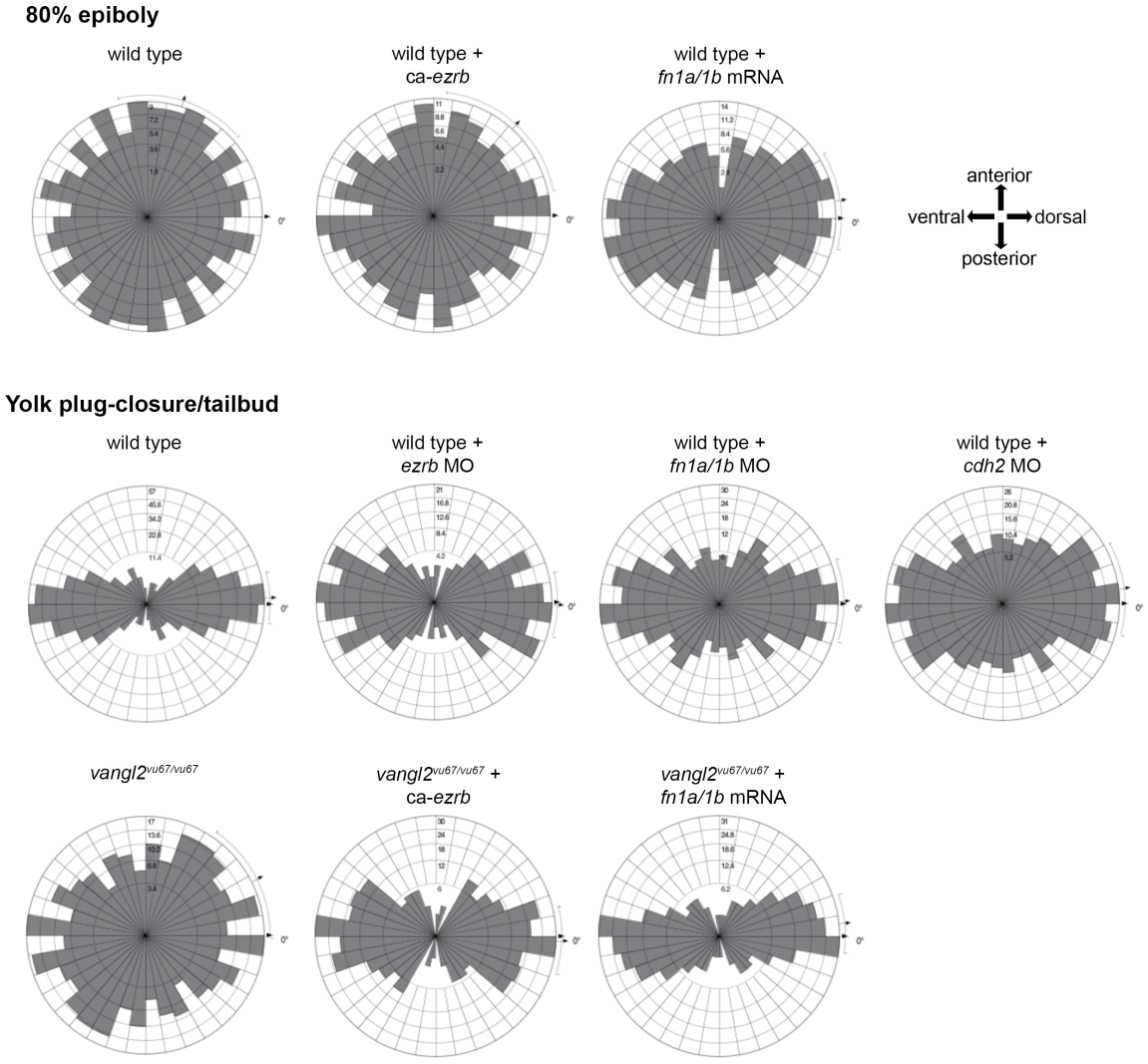

Fig. S8. *cdh2*$^{tm101/tm101}$ mutant embryos recapitulate *cdh2* morphant phenotypes. Twelve embryos from a *cdh2*$^{tm101/+}$ incross were randomly selected and subjected to DIC time-lapse imaging (5 min with 30 s sampling intervals). Each embryo was genotyped using PCR amplification of genomic DNA and sequencing. Homozygous *cdh2*$^{tm101/tm101}$ embryos have a T->A base-change at amino acid Tyr 514 that introduces a stop codon (Lele et al., 2002). (A) Genotyping results. (B) Representative images from our time-lapse analyses. Images shown are separated by 30 s time intervals and white arrows denote forming and retracting bleb protrusions. Images are oriented with anterior to the top and dorsal to the right. Scale bars, 5 μm. (C) Germline *cdh2* mutant embryos have defective PCP and greater mesodermal blebbing (*cdh2*$^{+/+}$ siblings and *cdh2*$^{tm101/tm101}$ mutants, n=50 cells for PCP analysis, n=280 cells for bleb analysis, 2 embryos per genotype). **P*<0.05, ****P*<0.001, *****P*<0.0001; unpaired Student's t-test with Welch's correction.

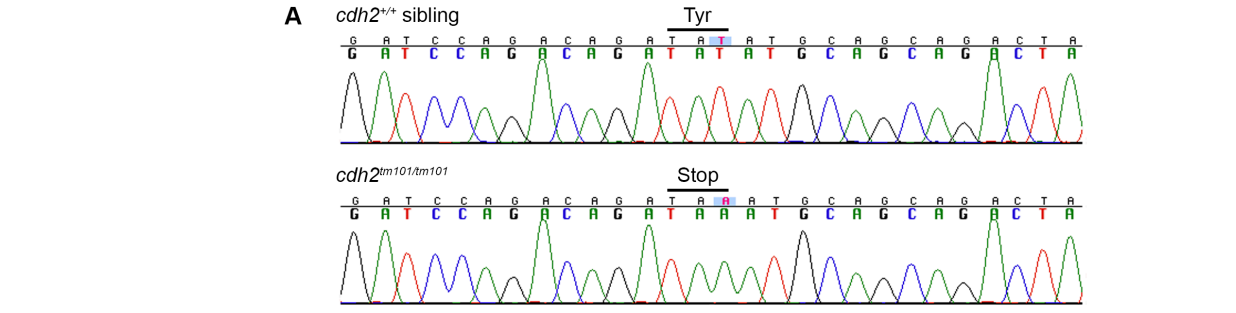

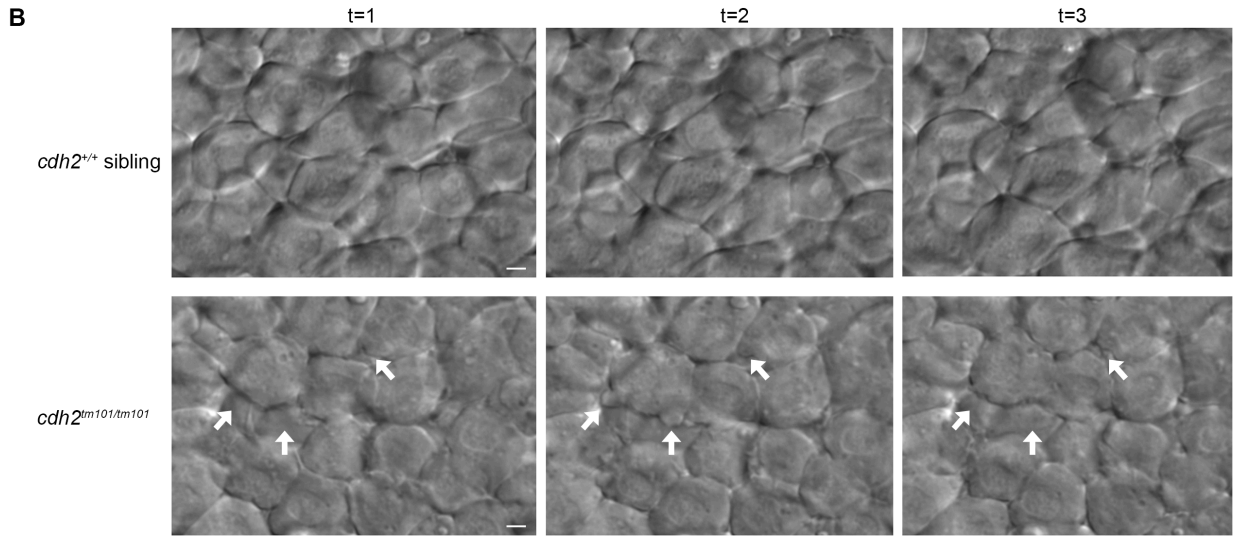

C

	LWR	MLA (% +/- 20°)	Cells forming blebs (%)	Total blebs
cdh2$^{+/+}$ sibling	1.49 +/- 0.25	72	1	3
cdh2$^{tm101/tm101}$	1.23 +/- 0.15****	38***	11*	31

Fig. S9. Western blot analysis showing Ezrb and Cdh2 knockdown. Representative blots of total protein extracts from ypc/tb stage *ezrb* and *cdh2* MO injected wild-type embryos (repeated two times). Blots were stripped and re-probed using a β-actin antibody. Relative densitometry values are indicated beneath each lane. The pan-cadherin antibody recognizes an epitope that is conserved between Cdh2 and E-cadherin (Cdh1).